Macromolecules

pubs.acs.org/Macromolecules Article

Predicting the Miscibility and Rigidity of Poly(lactic-*co*-glycolic acid)/Polyethylene Glycol Blends via Molecular Dynamics Simulations

Martina Pannuzzo,* Bruno A. C. Horta, Carmelo La Rosa, and Paolo Decuzzi

Cite This: *Macromolecules* 2020, 53, 3643−3654 Read Online

ACCESS | Metrics & More | Article Recommendations | Supporting Information

ABSTRACT: The addition of polyethylene glycol (PEG) chains to poly(lactic-*co*-glycolic acid) (PLGA) matrices is extensively used to modulate the biodegradation, drug loading and release, mechanical properties, and chemical stability of the original system. Multiple parameters, including the molecular weight, relative concentration, polarity, and solubility, affect the physicochemical properties of the polymer blend. Here, molecular dynamics simulations with the united-atom 2016H66 force field are used to model the behavior of PLGA and PEG chains and thus predict the overall physicochemical features of the resulting blend. First, the model accuracy is validated against fundamental properties of pure PLGA and PEG samples. In agreement with previous experimental and theoretical observations, the PLGA solubility results to be higher in acetonitrile than in water, with Flory parameters $\nu_{ACN} = 0.63 \pm 0.01$ and $\nu_{W} = 0.21 \pm 0.02$, and the Young's modulus of PLGA and PEG equal to $Y = 2.0 \pm 0.43$ and 0.32 ± 0.34 GPa, respectively. Next, four PEG/PLGA blending regimes are identified by varying the relative concentrations and molecular weights of the individual polymers. The computational results demonstrate that at low PEG concentrations (<8% w/w), homogeneous blends are generated for both low and high PEG molecular weights. In contrast, at comparable PEG and PLGA concentrations (∼50% w/w), short PEG chains are only partially miscible whereas long PEG chains segregate within the PLGA matrix. This behavior has been confirmed experimentally via differential scanning calorimetry and is in agreement with previous observations. Finally, the computed Young's modulus of PLGA/PEG blends is observed to decrease with the PEG content returning the lowest values for the partial and fully segregated regimens ($Y \approx 1.3$ GPa). This work proposes a computational scheme for predicting the physicochemical properties of PLGA/PEG blends paving the way toward the rational design of polymer mixtures for biomedical applications.

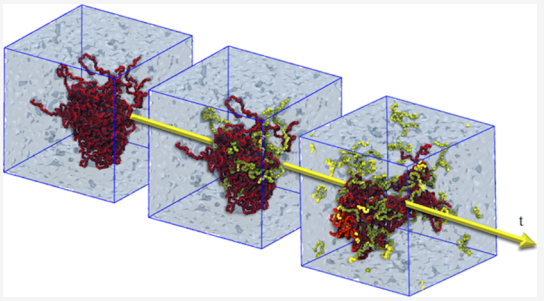

1. INTRODUCTION

Over the last decades, FDA-approved poly(lactic-*co*-glycolic) acid (PLGA) has been extensively employed in a variety of biomedical applications for its biocompatibility, biodegradability, and tunable mechanical and pharmacological properties.[1] PLGA has been formulated in nanoparticles, for the systemic delivery of small molecules and biologicals mostly against cancer and cardiovascular diseases, and in implantable devices, for the long-term and sustained release of therapeutic molecules to modulate chronic inflammation and support tissue regeneration.[2,3] Different approaches have been proposed to finely tune the biodegradation rates, drug-release profiles, glass transition temperatures, and other biophysical properties of pure PLGA nanoparticles and implants. These include the realization of PLGA block copolymers and PLGA blending with either natural or synthetic polymers.[4−6] Indeed, different from block copolymerization, mixing PLGA with other polymers to obtain blends does not require additional synthesis, purification, and characterization steps.

Focusing on blending, natural polymers, such as chitosan and collagen, have been mixed with PLGA to modulate release kinetics of both hydrophobic and hydrophilic drugs and improve the mechanical properties, such as muco-adhesiveness.[7,8] Synthetic polymers, such as polyethylene glycol (PEG), have been commonly used as additives to PLGA. For instance, Feng et al. generated, via nanoprecipitation, PLGA−based nanoparticles by blending together PLGA−PEG block copolymers and PLGA in order to accurately control the surface density of ligand molecules and thus enhance specific cancer cell targeting.[9] A similar approach was adopted by Hanes and collaborators to finely control the surface density of PEG on nanoparticles to enhance their permeation into mucus and brain tissues while modulating biodegradation and drug release kinetics.[10] PLGA−PEG blend nanoparticles were also shown to increase the bioavailability of curcumin molecules upon oral administration.[11] More recently, by mixing long PLGA chains (∼40 kDa) with short PEG chains (∼1 kDa), the authors have realized discoidal polymeric nanoconstructs with

Received: January 15, 2020
Revised: April 7, 2020
Published: May 12, 2020

https://dx.doi.org/10.1021/acs.macromol.0c00110
Macromolecules 2020, 53, 3643−3654

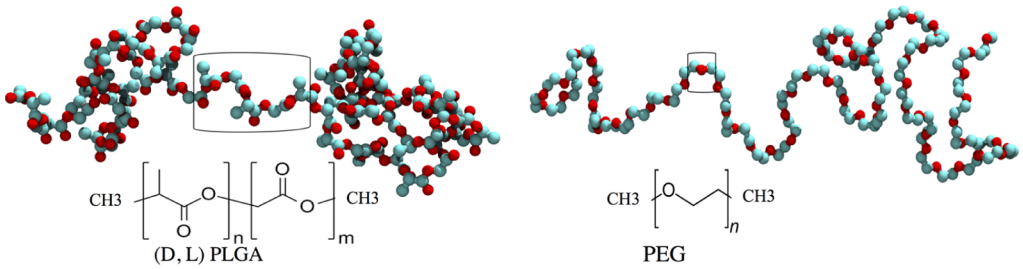

Figure 1. Definition of the molecular system. PLGA and PEG chemical structures.

controlled deformability (Young's modulus) and minimal macrophage sequestration.[12,13]

The realization of homogenous and stable polymer blends is challenging in that miscibility depends on several factors including the chemical composition, molecular weight, and relative concentration of the mixed polymers. As such, differences in experimental and synthesis conditions lead to polymer blends with very different physicochemical properties. Focusing on PLGA−PEG mixtures, other authors have shown that PLGA (68 kDa) and PEG (1 kDa) can homogenously mix only above the crystal-melting temperature of PEG (~30 °C), for solutions with comparable polymer concentrations.[14] Using coherent anti-Stokes Raman scattering (CARS) microscopy, other authors have demonstrated that PLGA (44 kDa) and PEG (2 kDa) start to segregate already at 10% weight percentage of PEG and that the PEG enriched phase appears as small islands within the PLGA matrix.[15] More recently, the authors have shown that the addition of small amounts of PEG (0.7 kDa) to PLGA (44 kDa) can effectively modulate the rigidity over the entire polymer blend, as measured via atomic force microscopy, suggesting that the two species are properly mixed at room temperature.[13] In such a complex scenario, computational modeling could help to identify key regulating factors and unravel the complex relationship between polymer composition, molecular weight, and relative concentration with the physicochemical properties of the mixture. Interestingly, while PEG has been extensively modeled in the literature using different approaches and force fields, minimal work has been devoted to simulate the molecular behavior of PLGA.[16]

In this work, molecular dynamics simulations relying on the united-atom 2016H66 force field are proposed for modeling the behavior of PLGA and PEG, alone and in the form of mixtures.[17] First, the accuracy of the force field is tested against experimental single PLGA and PEG fundamental properties, such as the radius of gyration in different solvents (acetonitrile and water), the polymer chain persistence length, and the Young's modulus. PLGA and PEG chains with molecular weights ranging from several hundreds to a few thousands of Daltons are considered. Then, the proposed computational approach is employed to study the miscibility of PLGA and PEG under different regimens, depending on the polymer relative concentrations and molecular weights. Results from simulations are validated against experimental data generated via differential scanning calorimetry (DSC) and already available in the open literature. Finally, the Young's modulus of PLGA−PEG blends is examined under different mixing regimens.

2. METHODS AND MATERIALS

2.1. Definition of the Molecular Systems. Molecular topologies for both PLGA and PEO were constructed according to the definitions of the united-atom 2016H66 forcefield.[17,18] This was shown to accurately reproduce the liquid properties and solvation free energies of several compounds, including alcohol, ether, aldehyde, ketone, carboxylic acid, ester, amine, amide, thiol, sulfide, and disulfide, as well as aromatic compounds and nucleic-acid bases. In the present work, ether and ester parameters were used to construct the topology of a PLGA polymer chain, whereas the vicinal diether parameters were used to model the PEO polymer chain.[19]

PLGA is a copolymer of lactic acid (LA) and glycolic acid (GA). LA contains an asymmetric α-carbon and its stereochemistry is typically defined in terms of the Fischer configuration, D or L. Randomly distributed atactic or syndiotactic PLGA is obtained by the standard use of the ring-opening polymerization technique.[20] The syndiotactic version of PLGA, presenting the same GA and LA monomer ratio (LA/GA 50:50), with D- and L-forms of LA alternately distributed, was considered here (see Figure S1a for the topology of PLGA). Thus, in the extreme limit of a low degree of polymerization, an even statistical presence of both GA and LA blocks and L,D-LA stereoisomers was guaranteed. The dimeric unit (L,LA−GA-D,LA−GA) of PLGA was replicated to obtain chains with degree of polymerization DP = 16, 37, 64, and 87 corresponding to a molecular weight (MW) of 1.084, 2.367, 4.204, and 5.463 kDa, respectively. In the case of PEO, the unit (C−O−C) was replicated to obtain chains with degree of polymerization DP = 16, 37, 64, and 87 corresponding to MWs of 0.706, 1.630, 2.818, and 3.830 kDa, respectively. In both cases, the chains were terminated with methyl groups to reduce the influence of both ends on the average behavior of the chain (Figure 1). Despite their different termini, PEO and PEG behave similarly in the limit of high DP.[19] From now on, for simplicity, we will refer to PEO chains as PEG throughout the rest of the manuscript. At atomistic resolution, the simulation of short chains is preferred to guarantee shorter equilibration times and avoid chain entanglement, which may significantly affect the Young's modulus:[21] For PEG melts, entanglement originates at a critical polymer molecular weight MW_c of 3−4 kDa.[22] For PLGA, the entanglement probability is poor at MW_c below 7 kDa.[23] As such, PLGA and PEG chains were first randomly distributed and assembled at low density within a cubic box. A simulated annealing run, from 500 to 300 K at a rate of 1 K ns^{-1}, allowed for the polymer chain relaxation and box compression. Each system was further equilibrated at 300 K until the system density no longer drifted. After equilibration, single polymer samples and binary mixtures (PLGA and PEG together) were simulated at 500 K for 300 ns and 1 μs, respectively, to allow for proper equilibration.[24] Note that 500 K is well above the glass transition temperature for PLGA and PEG. Final configurations at 500 K were annealed down to 300 K at a rate of 10 K ns^{-1} and simulated for further 300 ns.

2.2. Simulation Details. All simulations were performed using the GROMACS program (version 5.1.4)[25] along with the 2016H66 forcefield.[17] Systems were equilibrated using a Berendsen weak-coupling thermostat and barostat algorithms.[26] The equations of motion were integrated using the leapfrog algorithm with a timestep of 2 fs.[27] In the production run, the temperature was controlled using a velocity-rescale thermostat[28] with a time constant of 0.1 ps and a reference temperature of 300 or 500 K, depending on the system under investigation. Periodic boundary conditions were applied. The Parrinello−Rahman algorithm was applied for isotropic pressure coupling (1 bar).[29] The Verlet cut-off scheme was used for the

https://dx.doi.org/10.1021/acs.macromol.0c00110
Macromolecules 2020, 53, 3643−3654

construction of pairlist. Coulomb interactions were calculated using the PME (Particle−Mesh−Ewald) method with a cutoff radius set to 1.4 nm, Fourier spacing of 0.12 nm, and cubic interpolation. The van der Waals interactions were evaluated using a single cut-off of 1.4 nm. Although this procedure is different from the original one used in the force field parametrization, a systematic investigation was carried out to demonstrate that the present setup is valid and preferable when using GROMACS software.[30] In order to test the validity of these setup parameters, the density of 1,2-dimethoxyethane (DXE) was calculated and shown to successfully reproduce the value obtained in the original work.[19]

2.3. Trajectory Analysis. *2.3.1. Hildebrand Solubility Parameter.* The Hildebrand solubility parameter, δ, is used to predict the solubility of polymers in a solvent solution or the compatibility of two different polymers.[31] The parameter δ is defined as

$$\delta = \sqrt{\frac{E_{coh}}{V_M}} \tag{1}$$

where E_{coh} is the intermolecular interaction energy, $V_M = \frac{M}{\rho}$ is the system molar volume, where M the molar mass and ρ is the system density. The ratio $\frac{E_{coh}}{V_M}$ is the cohesive energy density, which corresponds to the intermolecular attraction energy per unit volume in pure substances.[32] The value for E_{coh} is derived via MD simulations according to the formula[33]

$$E_{coh} = \sum_{chains} E_i - E_{tot} \tag{2}$$

where E_i is the potential energy of individual polymer chains and E_{tot} is the total potential energy of the system.

A protocol similar to that described by Glova et al.[24] was followed for the extrapolation of E_i from the MD simulations, as detailed in the sequel. First, the MD trajectory was converted into separate trajectories for each individual chain i in the system, using the GROMACS routine "gmx mdrun −rerun". Then, the potential energies of the isolated chains, as well as the total potential energy E_{tot} of the system, were estimated over time using the GROMACS routine "gmx energy". Finally, the intermolecular interaction energy E_{coh} was derived according to eq 2, from which the solubility parameter was then estimated according to eq 1.

The values of δ for pure PLGA or PEG were calculated for two different chain lengths (DP = 16; 64) and every 100 ns over temporal windows of 100 ns each. Because the experimental glass transition temperature T_g for PLGA is near the body temperature (~310 K),[34] the material may be in a different physical state and have completely different properties before and immediately after administration in the body. Therefore, the value of δ was also extrapolated below and above the estimated T_g for PLGA, specifically at 300 and 500 K. Furthermore, the value of δ was also computed by performing simulations with different box sizes (different number of chains) in the case of PEG, to characterize the finite size effects on δ.

2.3.2. Single Chain Properties: Radius of Gyration, Solubility, and Persistent Length. The behavior of polymer solutions can be discussed within the framework of Flory−Huggins theory. This theory predicts that the gyration radius R_g of the polymer chains follows the relationship $R_g \approx DP^{\nu}$, where DP is the number of monomers per chain (degree of polymerization) and the exponent ν is related to the behavior of the polymer chains in solution. Specifically, for energetically favorable solute−solvent interactions that promote polymer swelling, $\nu = 3/5$ (good solvent conditions); when solute−solute interactions prevail causing the contraction of the polymer coils, $\nu = 1/3$ (bad solvent conditions); if the solute−solute and solute−solvent interactions are comparable, $\nu = 1/2$ (Θ conditions).[35] The gyration radius R_g is defined and computed as the root mean square of the distance of all N atoms of the polymer chain from their center of mass (CoM) according to

$$\langle R_g^2 \rangle^{1/2} = \frac{1}{N}\sum_{i=1}^{N} (r_i - r_{CoM})^2 \tag{3}$$

where the angular brackets ⟨...⟩ denote the mean over the polymer molecules of the sample, and over the time. Thus, the exponent ν of the Flory−Huggins relation $R_g \approx DP^{\nu}$ was derived from calculating R_g through eq 3 above and correlating it with the number of monomers DP.

The persistence length P_l was calculated based on the (average) bond−vector autocorrelation function

$$C_{b,n} = (N-n)^{-1}\sum_{i=1}^{N}\sum_{j=1}^{N} \delta_{i+n,j}\langle \boldsymbol{u}_i \cdot \boldsymbol{u}_j \rangle \tag{4}$$

where δ is the Kronecker delta function, N is the number of covalent bonds along the polymer backbone, u_i and u_j are unit vectors along the ith and jth bonds, and n (in the limit between 0 and $N-1$) is the bond-order of the correlation, with the particular case $C_{b,0} = 1$.

In polymer theory, the above autocorrelation function $C_{b,n}$ is expected to follow an exponential decay with respect to n

$$C_{b,n} = e^{-n_p^{-1} n} \tag{5}$$

where the persistence number n_p is a quantity that depends on the polymer type and experimental conditions. The value of n_p is calculated from the simulations based on the (average) autocorrelation functions $C_{b,n}$ for n even, as the intercept of a least-squares-fit line to the graph of ln $C_{b,n}$ against n with a horizontal line at −1.

The corresponding value of the persistent length P_l is then derived according to the expression

$$P_l = l_b n_p \tag{6}$$

where l_b is a representative covalent bond length along the polymer backbone. In this work, it was chosen as the average bond length between a C−O and a C−C bond ($l_b \approx 1.48$ Å).[19]

2.3.3. Young's Modulus. The ability of materials to deform under load is generally characterized through the Young's modulus Y. Within the small deformation regime, this modulus is defined as the ratio between the stress σ and the corresponding strain ε

$$Y = \frac{\sigma}{\varepsilon} = \frac{\frac{F}{A}}{\frac{\Delta L}{L_o}} = \frac{F}{\Delta L} \times \frac{L_o}{A} \tag{7}$$

where ΔL is the uniaxial elongation (or contraction) over the initial length L_o; F is the force exerted; and A is the cross-sectional area in the direction orthogonal to the applied force. In order to calculate Y, following a previously standardized procedure,[21,36] the simulated system was axially deformed at a constant rate of 10^{-4} nm ps^{-1} at 300 K. In the direction of the applied deformation, the box compressibility was set to zero, while in the other two transversal directions compressibility was set to 4.5×10^{-5} bar^{-1}. As a consequence, the box elongated along the loading direction and shrunk along the two normal directions, under an applied external pressure of 1 bar. During the deformation process, the elements of the pressure tensor P_i ($i = x, y, z$) and the simulation box size L_i were saved every 1 ps and converted into stress and relative strain according to the relations $\sigma = -P_i$ and $\varepsilon = \frac{\Delta L_i}{L_{0i}}$, respectively. According to eq 7, the Young's modulus Y was then calculated from the slope of the stress−strain curve, considering a linear fitting up to 2% of deformation (elastic regime), where the stress increases linearly with the strain. The values calculated at 3 different times (every 100 ns) and along the three directions (x, y, and z axis) were averaged out to give $\overline{Y}$.

2.3.4. Flory Parameter. According the Flory−Huggins theory, the mean free energy change per unit volume upon mixing is given by

$$\frac{\Delta f}{k_B T} = \frac{\phi_A}{DP_A}\cdot\ln(\phi_A) + \frac{\phi_B}{DP_B}\cdot\ln(\phi_B) + \phi_A\cdot\phi_B\cdot\chi \tag{8}$$

https://dx.doi.org/10.1021/acs.macromol.0c00110
Macromolecules 2020, 53, 3643−3654

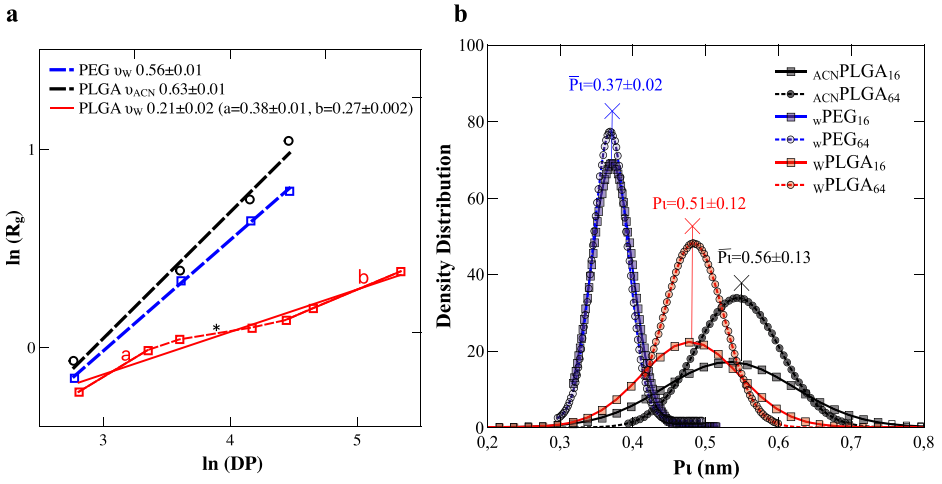

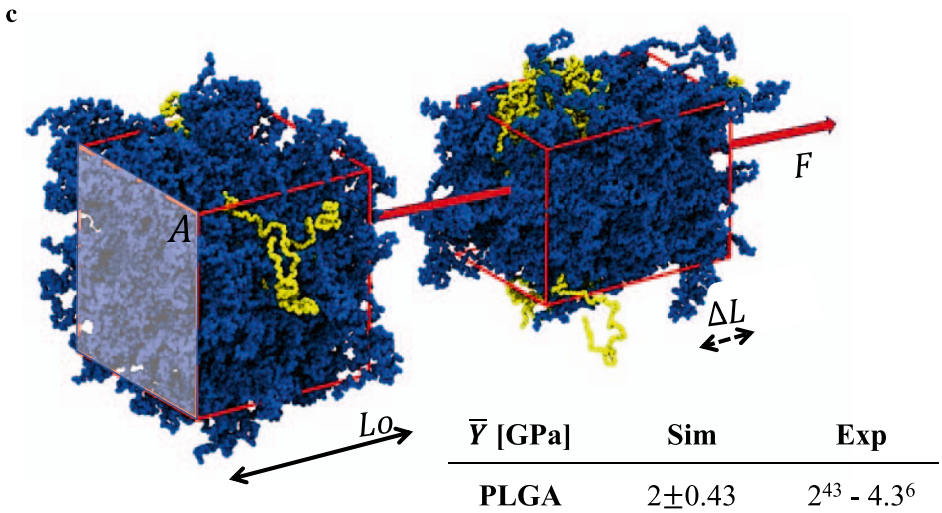

$\bar{Y}$ [GPa]	Sim	Exp
PLGA	2±0.43	2[43] - 4.3[6]
PEG	~0.32±0.34	0.22[45]

Figure 2. Pure polymer case: validation of the computational model. (a) Radius of gyration R_g as a function of the degree of polymerization DP for PEG in water (blue profile) and PLGA in acetonitrile (black profile) and water (red profile). The exponent υ in the relationship $R_g \approx DP^{\upsilon}$ coincides with the slope of the two square-fitted lines. (b) Distributions of the persistence lengths computed over 100 ns of simulations for PEG chains in water (blue) and PLGA chains in acetonitrile (black) and water (red) and two different degrees of polymerization (full line for DP = 16 and dashed line for DP = 64). (c) Simulation box and 3D representation of the axial deformation of a polymeric box subjected to a force F for calculating the Young modulus Y. In the table, values of the Young's modulus Y are estimated via the proposed Molecular Dynamics approach (*Sim*) and compared with experimental data (*Exp*) available in the literature.

where ϕ_A and ϕ_B are the volume fractions of the two polymer species A and B in the blend; DP_A and DP_B represent the degrees of polymerization (or number of monomers) for the two species; χ is the dimensionless Flory–Huggins interaction parameter; T is the absolute temperature; and k_B is the Boltzmann constant ($k_B = 1.380 \times 10^{-23}$ J K^{-1}). The first two terms on the right hand side of eq 8 account for the entropy of mixing, which decreases with the molar mass (~$DP_{A,B}$) of the mixing species. The third term is the enthalpy of mixing, which depends on the strength of the solvent–solvent, polymer–solvent, and polymer–polymer intermolecular interactions through a unique mean–field parameter χ. The critical value χ_{cr} of the Flory–Huggins interaction parameter required for the demixing of the polymer mixture obeys the following equation

$$\chi_{cr} = \frac{1}{2}\cdot\left(\frac{1}{\sqrt{DP_A}} + \frac{1}{\sqrt{DP_B}}\right)^2 \quad (9)$$

Therefore, two polymers blend together if the interaction parameter χ is lower than the critical value χ_{cr}. The Flory–Huggins interaction parameter χ is defined as the ratio between the total interaction energy and the thermal energy $R{\cdot}T$

$$\chi = \frac{\Delta E_{mix}\cdot V_{mono}}{R\cdot T\cdot \phi_A\cdot \phi_B} \quad (10)$$

where $\Delta E_{mix} = \phi_A(\delta_A)^2 + \phi_B(\delta_B)^2 - \delta_{blend}$ is the internal energy change associated with blending; ϕ_A and ϕ_B are the volume fractions of A and B in the blend; δ_A and δ_B are the solubility parameters of the pure components A and B, respectively; and δ_{blend} is the solubility parameter of the A–B blend; T is the absolute temperature; and R is the universal gas constant (R = 8.314 J mol^{-1} K^{-1}). The term $V_{mono} = \frac{V_{blend}}{Q}$ is the molar volume of the repeat unit chosen as reference in a blend, V_{blend} is the molar volume of a blend, and Q is the number of monomers in a blend.

2.4. DSC Analyses of the Polymer Samples. The thermal properties of the pure polymer samples and binary mixtures were investigated by scanning differential calorimetry (DSC).[37] The instrument measures the specific heat of the material at constant pressure (C_p). In this technique, the sample is exposed to controlled heating/cooling cycles. First-order and second-order transitions can be readily detected. According to the classical Ehrenfest classification scheme, C_p assumes an infinite value (e.g., melting) at a first-order

https://dx.doi.org/10.1021/acs.macromol.0c00110
Macromolecules 2020, 53, 3643–3654

transition temperature, whereas C_p experiences an abrupt change in value at the second-order transition temperature[38,39] Although glass transition cannot be simply interpreted as a second-order transition,[40] it does appear as such in curves derived by calorimetric analyses.

Each sample was investigated using two heating/cooling thermal cycles, from 20 to 80 °C. Heating/cooling runs were performed with a rate of 1 °C/min. A 5 mg sample was sealed into an aluminum pan and scanned under nitrogen flow (30 L/h). In order to qualitatively identify the presence of different phases, the deconvolution of the C_p profile was performed using Gaussian curves. Considering that there is no theory on the deconvolution of the components in phase transitions, the following reasonable criteria was used: the minimum number of Gaussian curves was chosen to fit the C_p profile and the transition temperatures of each component were assigned at the individual peaks of the decomposed profile. The glass transition temperature (T_g) was calculated as the absolute maximum of the first derivative, corresponding to the midpoint of DSC thermograms. Further experimental details can be found in previous works.[41] All measurements were averaged over three independent analyses.

2.5. Statistical Analysis. Comparison of $\bar{Y}$ computed in different conditions was carried out by one way Anova. Significant statistical differences correspond to $p < 0.05$. The analysis was carried out using Prism "Graphpad" software.

3. RESULTS

3.1. Pure Polymer Case: Validation of the Computational Model. The behavior of pure PEG and pure PLGA solutions was studied under different conditions and compared with computational and experimental data available in the literature. The topology of poly(lactic-*co*-glycolic acid) (PLGA) and the chemical structures of PLGA and PEG are presented in Figures 1 and S1. Specifically, the following polymer samples were considered: PEG_{16}, consisting of 1,518 PEG chains with a degree of polymerization DP = 16; PEG_{64}, consisting of 368 PEG chains with DP = 64; $PLGA_{16}$, consisting of 972 PLGA chains with DP = 16; and $PLGA_{64}$, consisting of 243 PLGA chains with DP = 64. After reaching equilibration, the densities of these single polymer samples were observed to oscillate around 1.217 and 1.236 kg/m^3 for $PLGA_{16}$ and $PLGA_{64}$; 1.032 and 1.056 kg/m^3 for PEG_{16} and PEG_{64}, respectively.

To characterize the interaction of the polymer with a specific solvent, the radius of gyration of single PEG and PLGA chains was calculated and analyzed as a function of the molecular weight (DP = 16, 37, 64, and 87), in water and acetonitrile at 300 K, for 100 ns. The swelling behavior of the two polymers was estimated according to the Flory theory, as detailed in Section 2.3.2. Figure 2a shows the variation of the radius of gyration R_g for PEG in water (blue profile) and PLGA in acetonitrile (black profile) and water (red profile) as a function of the degree of polymerization DP, calculated via eq 3 in Section 2.3.2. Recalling that the radius of gyration increases with the degree of polymerization following the relationship $R_g \approx DP^{\nu}$, the exponent ν can be readily estimated by a least-square fitting of the data presented in Figure 2a. Specifically, for PEG in water, $\nu = 0.56 \pm 0.01$, indicating good solubility. This value is in good agreement with the experimental data ($\nu = 0.56 \pm 0.01$[19] and 0.58 ± 0.03[19]) and previous computational results ($\nu = 0.61$[19,42]). For PLGA in acetonitrile, $\nu = 0.63 \pm 0.1$, indicating good solubility. In contrast, for PLGA in water, $\nu = 0.21 \pm 0.02$, confirming that water is a poor solvent for this polymer. The ln R_g (ln DP) profile shows an inflection point for DP = 37 (c* red curve, Figure 2a) and ν is lower than the expected 1/3. This should be related to the fact that the law for the Flory exponent holds strictly in the so-called "scaling regime" or in other words in the limit of very long polymer lengths.[43] However, for the polymer molecular weights considered in this work, a significant finite-size effect would come into play. Consequently, as theorized for the theta regime, the conformation of a polymer would depend on its size: a globular form is associated with long polymeric chains, whereas a coil form is associated with short polymeric chains.[44,45] Indeed, the crossover between the two behaviors would be confirmed by the present simulations: for DP below c*, $\nu_a = 0.38 \pm 0.01$; for DP above c*, $\nu_b = 0.27 \pm 0.002$. In the limit of very long polymer chains, ν is expected to approach the value of 1/3. Experimental data would further support these observations in that PLGA solubility in water dramatically worsens above a certain size as it is well accepted that PLGA oligomers smaller than 1,100 g/mol are water soluble.[46] Both values of ν for PLGA in water and acetonitrile are in line with experimental polymer−solvent interactions measured by inverse gas cromatography (IGC).[47,48]

In addition to the radius of gyration, the persistence length P_l was also estimated for the PEG and PLGA chains (Figure 2b), following the methods described in Section 2.3.2. Given that P_l differs under Θ conditions as compared to a good solvent,[49] the persistence length of PLGA was computed in both acetonitrile and water and compared to that of PEG in water ($P_l = 0.37 \pm 0.02$ nm in good accordance with previous findings ($P_l = 0.37 \pm 0.04$ nm) (Figure 2b).[50] For PLGA, the persistence length was larger in acetonitrile ($P_l = 0.56 \pm 0.13$ nm) than in water ($P_l = 0.51 \pm 0.12$ nm) (Figure 2b). The molecular weight of the polymer chains had no significant effect on the persistence length. These results agree with the notion that pi bonds in PLGA contribute to the rigidity of the chains, whereas sigma bonds in PEG confer a higher flexibility to the chains.

Finally, the deformability of the pure polymer samples was also predicted. The Young's modulus Y for each pure polymer sample was quantified following the procedure described in the Section 2.3.3. The values of the Young's modulus calculated at 3 different times (every 100 ns) and along the three directions (x, y, and z axis) were averaged out to return the final Y value. A representation of the computational setup for the deformability test is given in Figure 2c. Similarly to the persistence length case, polymer chains with two different molecular weights were considered for both PEG and PLGA (DP = 16; 64). For PEG_{16} and PEG_{64}, $Y = 0.35 \pm 0.16$ and 0.40 ± 0.09 GPa, respectively (see Table in Figure 2c; Tables S1 and S2 for the full data set). The experimental data for PEG are scarce but, for 600 kDa PEG, the experimental Young's modulus value was measured to be 0.22 GPa.[51] Also, using atomic force microscopy, the Young's modulus of a 100 kDa PEG was found to be 0.2 GPa.[52] Although these experimental values were obtained under different experimental conditions, and considering PEG chains of different molecular weights, it is comforting to see that they still return Young's moduli close enough to the present computational estimates. For $PLGA_{16}$ and $PLGA_{64}$, $Y = 2.38 \pm 0.35$ and 1.98 ± 0.74 GPa, respectively (Table in Figure 2c; Tables S1 and S2 for the full data set). These computed values of the Young's modulus are in good agreement with the experimental data derived using different loading setups. Specifically, in a conventional tensile test, PLGA films returned a Young's modulus of 3.5 ± 0.2 GPa; in a nanoindentation test, a modulus of 3.8 ± 0.1 GPa was measured;[53] employing an ultrasonic technique, a PLGA shell provided a $Y = 4.3$ GPa;[54] force microscopy measure-

https://dx.doi.org/10.1021/acs.macromol.0c00110
Macromolecules 2020, 53, 3643−3654

a

SYSTEM	PEG:PLGA	DP	Number of chains	
		PEG	PEG	PLGA
A (8% PEG_{16})	8:92	16	108	243
B (8% PEG_{64})	8:92	64	27	243
C (46% PEG_{16})	46:54	16	500	125
D (46% PEG_{64})	46:54	64	125	125

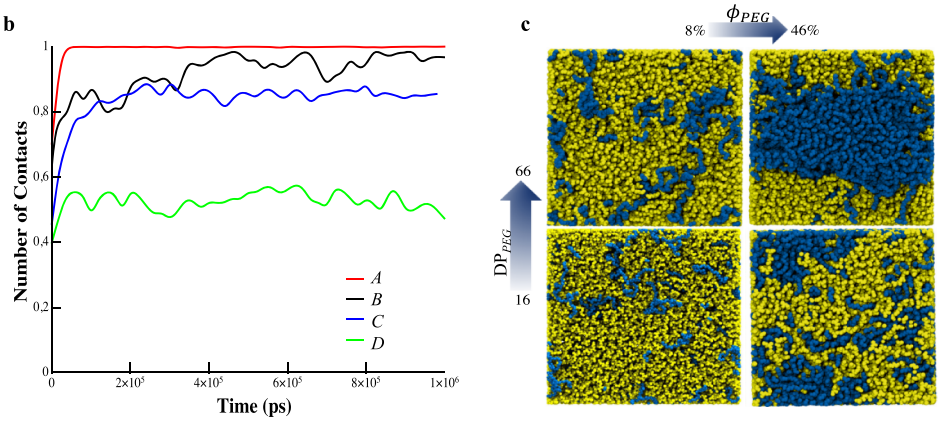

Figure 3. Binary mixture: PLGA and PEG miscibility. (a) List of the binary mixtures simulated. (b) Temporal variation of the number of PLGA−PEG intermolecular contacts computed over 1 μs of simulation and normalized by the number of PEG atoms: For *system A* (red line), *N* reaches a steady-state value of 1 after about 1.3×10^5 ps; for *system B* (black line), *N* reaches a steady-state value of ∼0.95 after about 4×10^5 ps; for *system C* (blue line), *N* reaches a steady-state value of ∼0.82 after about 2×10^5 ps; and finally for *system D* (green line) *N* reaches a steady-state value of only ∼0.5 after about 2×10^5 ps. (c) Snapshots of the system at 1 μs for the four different systems.

ments on PLGA structures returned a Young's modulus of about 2.4 GPa.[55] It is important to recall that other authors have already demonstrated via MD simulations that the Young's modulus *Y* only weakly depends on the degree of equilibration and the molecular weight of the polymer in regimes where size scales do not exceed the entanglement length.[21] Indeed, this observation is supported by the experimental evidence above and by the computational data presented in the Tables S1 and S2. Also, when comparing simulations with experiments, it should be kept in mind that the coarse graining of the hydrogens would reduce intermolecular friction and possibly underestimate Young's modulus *Y*. Also, the strain rates used in MD simulations are much larger than those applied experimentally, and this, on the other hand, would tend to overestimate the apparent Young's modulus.

3.2. Binary Mixture Case: Predicted PLGA and PEG Miscibility. PEG and PLGA were mixed together at two different ratios, namely, 8:92 and 46:54, and for two different degrees of polymerization, namely, DP = 16 and 64. This leads to four different binary mixture systems, as explicitly listed in Figure 3a. Notice that, at higher molecular weights (i.e.,: DP ≫ 64), the probability of the polymer chain entanglement would rapidly increase, slowing the dynamics down to a level not treatable with an atomistic description of the system.[56] *Systems A* and *B* correspond to a low PEG concentration (PEG/PLGA ratio 8:92) with PEG chains DP = 16 and 64, respectively. *Systems C* and *D* correspond to a high PEG concentration (PEG/PLGA ratio 46:54) with the PEG chains DP = 16 and 64, respectively. For all simulated systems, PLGA has a fixed DP = 64.

In order to verify that the equilibrium was successfully achieved within the binary mixture, the number of contact points *N* established between PLGA and PEG chains was monitored over time. A Gromacs routine "*gmx mindist*" was employed to estimate the number of contacts *N* between PEG and PLGA atom pairs within a distance $d = 0.6$ nm, which was then normalized by the total number of PEG atoms in the system. As expected, *N* grows with time up to a steady-state value—equilibrium condition (Figure 3b), which is reached at different time points depending on the molecular weight of the polymer chains. The parametric curves in Figure 3b demonstrate that at low PEG concentrations (*systems A* and *B*—8% PEG), the two polymers form a homogenous mixture, for both long and short PEG chains (PEG_{16} and PEG_{64}) combined together with long PLGA chains ($PLGA_{64}$), returning $N = 1$ and ∼0.95 at equilibrium, respectively. At higher PEG concentrations, the miscibility is significantly reduced. Miscibility is moderate for *system C* (46% PEG_{16}), returning $N \approx 0.82$; and poor for *system D* (46% PEG_{64}), returning $N \approx 0.5$. This is also graphically summarized by the four insets of Figure 3c, corresponding to the four tested systems, where the blue beads are for the PEG chains and the yellow beads are for the PLGA chains. At low PEG concentrations (left insets in Figure 3c), PEG/PLGA miscibility is good regardless of the PEG molecular weight. The yellow and blue beads are quite uniformly spread within the computational box. At high PEG concentrations (right

https://dx.doi.org/10.1021/acs.macromol.0c00110
Macromolecules 2020, 53, 3643−3654

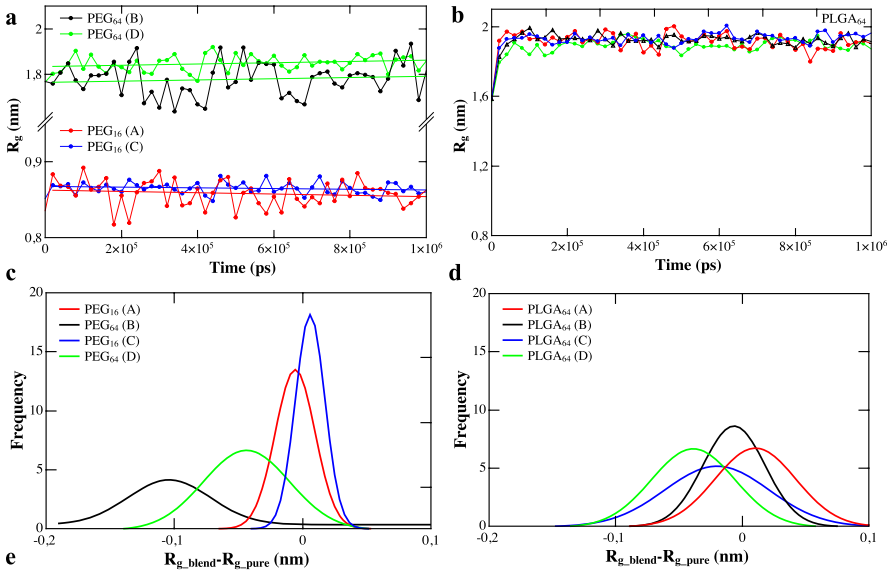

e

System	ϕ_{PEG}	ϕ_{PLGA}	N_B^{PEG}	N_B^{PLGA}	N_{chains}^{PEG}	N_{chains}^{PLGA}	δ_{blend} (J/cm^3)$^{1/2}$	χ_{cr}	χ
A	0.08	0.92	16	64	108	243	16.42	0.04	-0.68
B	0.08	0.92	64	64	27	243	16.40	0.02	-0.6
C	0.46	0.54	16	64	125	500	16.0	0.04	0.08
D	0.46	0.54	64	64	125	125	15.66	0.02	0.79

Figure 4. Binary mixture case: PLGA and PEG miscibility. (a) Gyration radius profiles of PEG chains of different molecular weights under different mixture compositions, (b) Gyration radius profiles for PLGA chains under different mixture compositions, (c) Gyration radius distribution of PEG chains normalized for the gyration radius of PEG in a pure sample; (d) Gyration radius distribution of PLGA chains normalized for the gyration radius of PLGA in a pure sample—*system A* (8:92 PEG_{16}:$PLGA_{64}$) in red; *system B* (8:92 PEG_{64}:$PLGA_{64}$) in black; *system C* (46:54 PEG_{16}:$PLGA_{64}$) in blue; *system D* (46:54 PEG_{64}:$PLGA_{64}$) in green. (e) Table listing the Flory parameter χ for the systems under study.

insets in Figure 3c), PEG/PLGA is partially miscible for low PEG molecular weight (PEG_{16}, see lower, right inset in Figure 3c), while segregation occurs with high molecular weight PEG (PEG_{64}, see upper, right inset in Figure 3c). In the case of partial miscibility, multiple blue and yellow areas can be identified within the computational box, where pure PLGA and PEG chains dominates. In the case of segregation, a large PEG domain can be readily identified in the inner zone of the computational box. For both the partially miscible and segregated cases, boundary areas at the interface between the pure PLGA and PEG phases can be identified where the two different polymers are in contact and interdigitated.

Furthermore, the radius of gyration R_g of the polymer chains was monitored over time for all mixtures under investigation. After a few nanoseconds, the gyration radius of the PEG chains stabilizes, with systems *A* and *B* showing more pronounced fluctuations. Specifically, for the low DP configurations (PEG_{16}), the average gyration radii were R_g = 0.86 ± 0.001 nm (red line; Figure 4a) and 0.85 ± 0.01 nm (blue line; Figure 4a) for *systems A* and *C*, respectively. Note that in pure PEG melts, the radius of gyration for PEG_{16} was R_g^{pure} = 0.86 ± 0.02 nm. For the high DP systems (PEG_{64}), the average gyration radii were R_g = 1.83 ± 0.03 nm (back line; Figure 4a) and 1.77 ± 0.07 nm (green line; Figure 4a) for the *systems B* and *D*, respectively. Note that in pure samples, the radius of gyration for PEG_{64} was R_g^{pure} = 1.9 ± 0.06 nm. The gyration radius of the PLGA chains did not vary with composition, returning similar values of R_g (~1.9 nm) for all four tested systems (Figure 4b). Note that in pure PLGA samples, the radius of gyration for $PLGA_{64}$ was R_g^{pure} = 1.93 ± 0.05 nm.

The difference between the gyration radii in the binary mixture R_g^{mix} and in the pure sample R_g^{pure} was estimated for all pure and mixture systems. Figure 4c,d shows such a difference ($R_g^{mix} - R_g^{pure}$) in the case of PEG and PLGA chains, respectively. In systems with a high degree of miscibility (i.e., *system A*), the radii of gyrations of both PEG_{16} and $PLGA_{64}$ chains remain unchanged, as compared to the pure polymer case (red curve in Figure 4c,d, respectively). For *system B*, the R_g of the PEG_{64} chains shifts to lower values (black curve, Figure 4c), whereas the R_g for the $PLGA_{64}$ chains remains unchanged (black curve, Figure 4d) as compared to the corresponding pure polymers. In this case, sparse PEG_{64} chains in contact with $PLGA_{64}$ appear less favored as compared to chains in the pure PEG_{64} sample, yet the two species remain miscible in the limit of a low amount of PEG_{64} in the mixture. In the case of poor miscibility (*system D*), R_g for both PEG_{64} and $PLGA_{64}$ chains shift to lower values (green curves, Figure 4c,d, respectively). In this case, chains of both types distributed at the interface of segregated domains become more compact so as to reduce their reciprocal contact area (reducing PEG-PLGA intermolecular interactions). Still, the R_g for the PEG_{64} chains is larger than that of PEG_{64} in *system B*. This is probably due to the dominant contribution to R_g of the more swollen chains within the segregated domain far from PLGA. Finally, the R_g values for both PEG_{16} and R_g $PLGA_{64}$ chains in *system C* are slightly perturbed (blue curve, Figure 4c,d, respectively), as

https://dx.doi.org/10.1021/acs.macromol.0c00110
Macromolecules 2020, 53, 3643−3654

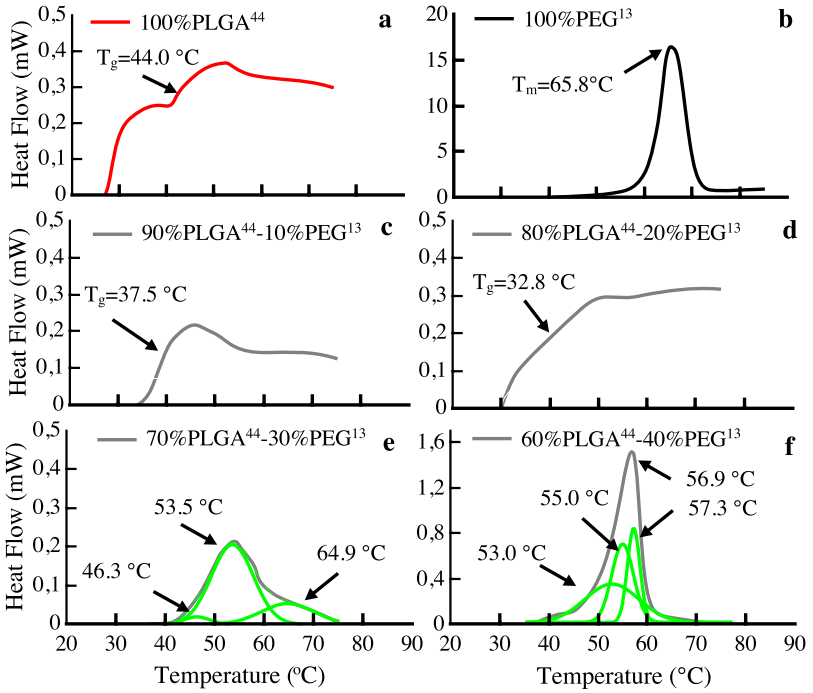

Figure 5. DSC measurements of the PLGA and PEG mixture. (a) T_g temperatures of pure 44 kDa PLGA; (b) solid−liquid phase transition of pure 13 kDa PEG; (c−f) heat-flow vs temperature diagrams for PLGA/PEG mixtures with a growing concentration of PEG from 10 to 40%. Panels e and f present the deconvolution of C_p profile for the PLGA/PEG mixture.

compared to the corresponding reference values. In this case, the less swollen $PLGA_{64}$ chains are more affected by of the abundant PEG_{16} chains as compared with system *A*, while the change in R_g of PEG_{16} chain is negligible for such a low molecular weight.

Another approach to assess the miscibility between the two polymers relies on the Flory−Huggins theory and the quantification of the Hildebrand solubility parameters δ for the two polymers.[24] Following the "like-dissolves-like" principle, miscibility occurs if the difference in the Hildebrand solubility parameters between the two polymers is smaller than 2 $(J/cm^3)^{0.5}$.[57,58] This would imply that attractive interactions between the two polymer chains are similar. Thus, the Hildebrand solubility parameters δ of the two polymer chains in the melt/solid state were derived following the methods described in Section 2.3.4. δ values calculated for the PLGA and PEG chains at different temperatures and degrees of polymerization are listed in the Tables S3 and S4. As expected, the estimated values of δ decrease as the temperature T increases.[59,60] At 300 K, the calculated δ was lower for pure PLGA (~20 $(J/cm^3)^{1/2}$) as compared to pure PEG (~21.50 $(J/cm^3)^{1/2}$). Based on these values, the difference in the solubility parameters between PEG and PLGA is very close to 2 $(J/cm^3)^{1/2}$, thus indicating again the miscibility of the two polymers.[61] Specifically, for PEG_{16} and $PLGA_{64}$ the δ difference is 1.99 $(J/cm^3)^{1/2}$; while for PEG_{64} and $PLGA_{64}$ the δ difference is 1.93 $(J/cm^3)^{1/2}$.

Another criterion for polymer miscibility is based on the quantification of the Flory−Huggins interaction parameter χ. If this parameter is lower than the critical value χ_{cr}, calculated by eq 9, the two polymers are miscible. Computed values for χ are listed in the table of Figure 4e. For *system A*, a $\chi = -0.68$ is significantly smaller than $\chi_{cr} = 0.04$, thus indicating the full miscibility of PEG_{16} and $PLGA_{64}$ chains. For *system B*, the interaction parameter χ is equal to −0.6 and is lower than the critical value $\chi_{cr} = 0.02$, and even in this case PEG_{64} with $PLGA_{64}$ chains mix. For *system C*, in which PEG_{16} and $PLGA_{64}$ chains only partially mix, the interaction parameter $\chi = 0.08$ is close to the critical value, $\chi_{cr} = 0.04$. Finally, for *system D*, where comparable amounts of PEG_{64} and $PLGA_{64}$ are present, phase separation occurs. In this case, $\chi = 0.79$ is above the critical value, $\chi_{cr} = 0.02$.

The same miscibility trend evidenced from the computed interaction parameter χ emerges from SAXS MD data reported in Figure S2.

To substantiate these results even further, the radial distribution function (RDF) profiles of PEG atoms in the proximity of PLGA atoms was also computed for the four tested systems. In Figure S3, the density of PEG atoms was plotted as a function of the distance from neighboring PLGA atoms. The overall density of PEG atoms near PLGA atoms is expected to depend on the relative compatibility of the two species. For a given PEG concentration, higher densities were observed for *system A* over *system B* (PEG_{16} vs PEG_{64}) and for *system C* over *system D* (PEG_{16} vs PEG_{64}). This continues to confirm the notion that short PEG_{16} chains are more prone to mixing with $PLGA_{64}$ than the long PEG_{64} chains, certainly due to entropic effects. However, the PEG concentration modifies the critical threshold of miscibility, boosting polymer demixing in PEG_{16}-enriched samples while PEG_{64} at low concentration is still miscible with $PLGA_{64}$.

3.3. Binary Mixture Case: Experimental PLGA and PEG Miscibility by DSC. In view of these results, the miscibility of PLGA and PEG chains would depend both on their relative concentrations and molecular weights. Miscibility is favored by low PEG concentrations and short PEG chains. This is in general agreement with the experimental data reported by other authors.[13,14] To complement the simulation data presented above, the miscibility range of high molecular weight PLGA chains with low molecular weight PEG chains

https://dx.doi.org/10.1021/acs.macromol.0c00110
Macromolecules 2020, 53, 3643−3654

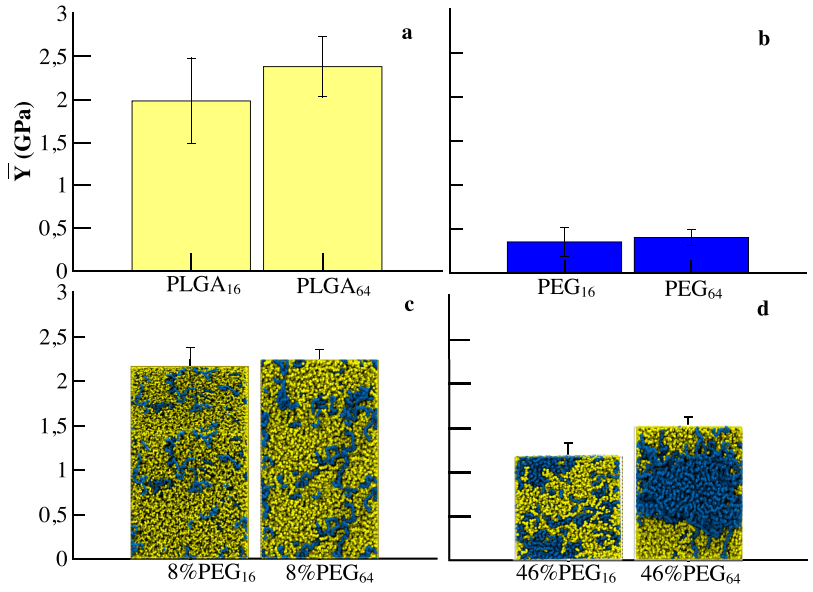

Figure 6. Young's Modulus of pure components and binary mixtures. (a) Young's Modulus of pure PLGA for two DP. (b) Young's Modulus of PEG for two DP. (c) Young's Modulus of binary mixtures of $PLGA_{64}$ and 8% PEG_{16} and 8% PEG_{64}. (d) Young's Modulus of binary mixtures of $PLGA_{64}$ and 46% PEG_{16} and 46% PEG_{64}.

was assessed via DSC. In particular, mixtures of 44 kDa PLGA chains (50:50 lactide/glycolide ratio) with 13 kDa PEG chains at different PLGA/PEG ratios, ranging from 0 to 100% PEG, were considered. In DSC, the amount of heat (heat flow) required to increase the temperature of a sample is measured as a function of the temperature, following specific heating/cooling cycles. Characteristic transition temperatures, such as the glass transition temperature T_g and the melting temperature T_m, can be extracted by the heat flow plots for pure samples and compared to that of the binary mixture. From this, information on the miscibility of the two polymers can be obtained.

Figure 5a,b presents the heat flow curves for pure PLGA and PEG samples, respectively. From Figure 5a, the glass transition temperature T_g of pure 44 kDa PLGA (50:50) is detected at 44 °C (see arrow). From Figure 5b, the melting temperature T_m of pure 13 kDa PEG is detected at 65.8 °C, corresponding to a well-defined, narrow peak. Figure 5c–f shows heat flow curves for PLGA/PEG mixtures with a PEG content of 10, 20, 30, and 40%, respectively. As the amount of PEG in the mixture increases, the shape of the curves changes within the considered temperature interval as well as the values of T_g and T_m. For PEG concentrations smaller than 30% (Figure 5c,d), a quasi linear reduction in the glass transition temperature is detected with T_g = 37.5 and 32.8 °C for a 10 and 20% 13 kDa PEG mixture, respectively. Also the overall shape of the heat flow curves is not affected by the presence of PEG. Thus, the presence of PEG affects the T_g of the mixture but not the overall behavior of the sample that still appears to be amorphous as pure PLGA. This would suggest that PLGA and PEG do mix homogeneously up to 20% PEG concentrations. In contrast, at PEG concentrations higher than 30% (Figure 5e,f), a more complex behavior is observed. Presumably, the T_g shifted to lower temperature values, which cannot be detected by the instruments, and broader melting peaks appeared. This would suggest the occurrence of phase segregation in the polymer mixture. The deconvolution of the heat flow curves, obtained as described in Section 2.4, allowed us to distinguish three components in the samples. For a 30% PEG content (Figure 5e), the component at 64.9 °C should be associated with a PEG phase enriched with some PLGA (enriched PEG), whereas the phases at lower temperatures would be much richer in PLGA. Increasing the concentration of PEG to 40% (Figure 5f), two cooperative phases and a very broad one were observed. The phases at high temperatures should be considered enriched in PEG.

In agreement with the DSC data, MD simulations of the binary PLGA/PEG mixtures did show segregation at high PEG concentrations (46%). The partial and total segregations can be graphically appreciated in the right insets of Figure 3c. Notice also that PEG–PLGA chains interdigitate at the interfaces between the phases (upper right corner in the panel of Figure 3c). Therefore, one can conclude that three regions coexist in the binary mixture at 40% of PEG[13] (Figure 5f): an enriched PLGA phase, which would correspond to the lower temperature transition; a PEG-enriched region, which would correspond to the transition at the highest T; and a region where PLGA and PEG chains interdigitate, which would correspond to the middle transition.

3.4. Binary Mixture Case: the Young's Modulus of PLGA and PEG Chains. Having established the conditions that would favor the proper mixing of PLGA and PEG chains, the Young's Modulus Y of the mixture was estimated. The computed Young's Modulus Y for the pure polymers and corresponding mixtures are provided in Figure 6.

Pure $PLGA_{16}$ and $PLGA_{64}$ samples returned a Y = 1.98 ± 0.74 and 2.38 ± 0.35 GPa (Figure 6a), respectively. Pure PEG_{16} and PEG_{64} samples returned a Y = 0.35 ± 0.16 GPa and 0.4 ± 0.09 (Figure 6b), respectively. While the Young's modulus of PLGA is about 1 order of magnitude higher than that of PEG, variations of Y with DP (16, 64) are statistically not significant. Indeed, it was previously noted that the molecular weight of the polymer has only a minor effect on its mechanical properties in regimes where size scales do not exceed the entanglement length.[21]

https://dx.doi.org/10.1021/acs.macromol.0c00110
Macromolecules 2020, 53, 3643–3654

In the case of mixtures, *system B* returned a Young's Modulus $Y = 2.27 \pm 0.11$ GPa, followed by a $Y = 2.16 \pm 0.21$ GPa for *system A*. No significant statistical difference was observed between these two systems and the pure PLGA case (Figure 6c). On the other hand, for comparable amounts of PLGA and PEG in the mixture, a significant drop in Young's modulus was observed (Figure 6d). Specifically, *system D* returned a Y value of 1.51 ± 0.11 GPa, compared to a value of Y 1.17 ± 0.16 GPa for *system C*. Indeed, the mixture is characterized by a lower rigidity as the PEG concentration increases (see Table S5 for the full data set). It is interesting to note that phase separation (formation of islands of PEG within a bulk PLGA matrix) is accompanied by a decrease in rigidity. However, in *system C*, the loss in rigidity is even larger in that the partial miscibility compromises more extensively the continuity of the bulk PLGA matrix and its resulting mechanical properties.

4. DISCUSSION

In biomedical applications, polymer blends are extensively employed to realize nano- and microparticles for the sustained delivery of therapeutic agents and macroscopic implants for tissue regeneration. The biodegradability, drug loading and release profiles, and the mechanical deformability of the polymer blends are fundamental features affecting the overall outcome of the medical intervention. In this work, a computational scheme is proposed to predict these features in terms of the polymer molecular weights and relative concentrations.

Focusing on PEG and PLGA, which are by far the most used polymers in biomedical applications, the addition of relatively small amounts of PEG (<10% w/w) to PLGA matrices still leads to quite homogeneous blends. This is graphically shown in Figure 3c, where the blue PEG chains are uniformly dispersed within the yellow PLGA matrix. At low PEG concentrations, miscibility is achieved for PEG chains with both low (DP = 16) and high (DP = 64) degrees of polymerization, corresponding to a molecular weight of 0.7 and 2.8 kDa, respectively. These miscibility studies were conducted for a fixed PLGA degree of polymerization (DP = 64), corresponding to a molecular weight of 4.2 kDa. Although the number of contact points N between PLGA and PEG chains at equilibrium is very close to 1 (i.e.: full miscibility—Figure 3b), small islands of PEG (blue) can still be identified within the PLGA (yellow) matrix. This has important implications to the field of drug delivery and tissue engineering as previous works have documented an augmented hygroscopicity of PEG-enriched PLGA matrices.[15,62] The increased permeation of water molecules deep inside the PLGA matrices can be associated with a faster release of hydrophobic agents. However, in terms of mechanical properties, no significant changes are observed with the addition of modest PEG amounts. However, this is shown only in the context of uniaxial rigidity (Young's modulus), under the assumption of small deformations (Figure 6). Other mechanical properties, such as the flexural rigidity, yield strength, tensile stress, and elongation at break will be analyzed in future works.

In contrast, the addition of PEG amounts comparable to that of PLGA (~50% w/w) is responsible for the formation of more heterogeneous blends with a level of phase separation that grows with the molecular weights of PEG. This is graphically shown in Figure 3c, where short PEG chains (bottom, right inset) form isolated blue inclusions within the yellow PLGA matrix. These inclusions are significantly larger than those observed at low PEG concentrations (left insets in Figure 3c). Under the partial miscibility conditions, drug release can be accelerated depending on the hydrophilicity of the therapeutic agent. Drug molecules can be partitioned and associated more avidly with one of the two phases, as shown in the case of paclitaxel by Kang and coworkers.[15] Furthermore, the Young's modulus decreases significantly down to 1.17 ± 0.16 GPa, which is close to the average value of pure PLGA (~2.2 GPa) and PEG (0.4 GPa). On the other hand, full segregation of the two phases is observed at high PEG molecular weight (top, right inset in Figure 3c). Under full segregation conditions, the chemical stability over time of the blend may not be guaranteed, as PLGA/PEG miscibility will change as the PLGA molecular weight decreases upon degradation, leading to a system that could rapidly release all its constituents and loose its mechanical properties.

These results could guide in tailoring the material stiffness of PLGA–PEG mixtures in terms of their miscibility and provide the rational basis for experimentally tuning polymer concentration[63] or molecular weight[13] in order to achieve the desired Young's modulus.

5. CONCLUSIONS

In summary, the present work provides computational tools for describing the molecular behavior of two extensively used polymers in the field of drug delivery and tissue engineering—PLGA and PEG. These tools can be accurately used to predict the miscibility of the two polymers and the pharmacomechanical properties of the resulting blends in terms of molecular weights, chemical structure, polarity, and relative concentration of the polymers. This computational scheme could certainly serve to optimize the behavior of polymer blends, avoiding extensive and costly experimental campaigns, and set the foundations for developing more efficient coarse-grained models of polymer blends.

■ ASSOCIATED CONTENT

Supporting Information

The Supporting Information is available free of charge at https://pubs.acs.org/doi/10.1021/acs.macromol.0c00110.

PLGA topology and forcefield parameters; averaged Young's modulus Y for PLGA as a function of the direction, DP, and time; averaged Young's modulus Y for PEG as a function of the direction, DP, and time; PEG Hildebrand solubility parameter; PLGA Hildebrand solubility parameter; SAXS profiles of neat homopolymers and binary mixtures; and radial density function profiles and averaged Young's modulus Y for PLGA/PEG mixtures as a function of the direction, DP, and time (PDF)

■ AUTHOR INFORMATION

Corresponding Author

Martina Pannuzzo − *Laboratory of Nanotechnology for Precision Medicine, Fondazione Istituto Italiano di Tecnologia, Genoa 16163, Italy;* orcid.org/0000-0001-8629-0173; Email: martina.pannuzzo@iit.it

https://dx.doi.org/10.1021/acs.macromol.0c00110
Macromolecules 2020, 53, 3643−3654

Authors

Bruno A. C. Horta − *Instituto de Química, Universidade Federal do Rio de Janeiro, Rio de Janeiro 21941-909, Brazil;* orcid.org/0000-0002-3952-1474

Carmelo La Rosa − *Department of Chemical Sciences, University of Catania, Catania 95125, Italy;* orcid.org/0000-0002-7123-5347

Paolo Decuzzi − *Laboratory of Nanotechnology for Precision Medicine, Fondazione Istituto Italiano di Tecnologia, Genoa 16163, Italy;* orcid.org/0000-0001-6050-4188

Complete contact information is available at: https://pubs.acs.org/10.1021/acs.macromol.0c00110

Author Contributions

M.P. performed all the simulations and analyzed the data. C.L.R. performed DSC experiments. P.D. was the originator of the idea underlying the actual research and wrote the manuscript. All the authors have contributed to the discussion and writing of the manuscript and approved its final version.

Notes

The authors declare no competing financial interest.

■ ACKNOWLEDGMENTS

This project was partially supported by the European Research Council, under the European Union's Seventh Framework Programme (FP7/2007-2013)/ERC grant agreement no. 616695, by the Italian Association for Cancer Research (AIRC) under the individual investigator grant no. 17664, by the European Union's Horizon 2020 research and innovation programme under the Marie Skłodowska-Curie grant agreement no. 754490-MINDED; and by the MAECI Italy-Serbia grant 2019 Prot. nr. MAE0057596. We acknowledge the CINECA award under the ISCRA initiative, for the availability of high-performance computing resources and support. The Brazilian agencies CAPES (Finance code 001), CNPq and FAPERJ, as well as the Núcleo Avançado de Computação de Alto Desempenho (NACAD/COPPE/UFRJ), and the Sistema Nacional de Processamento de Alto Desempenho (SINAPAD), are gratefully acknowledged.

■ REFERENCES

(1) Lee, B. K.; Yun, Y.; Park, K. PLA micro- and nano-particles. *Adv. Drug Delivery Rev.* **2016**, *107*, 176−191.

(2) Danhier, F.; Ansorena, E.; Silva, J. M.; Coco, R.; Le Breton, A.; Préat, V. PLGA-based nanoparticles: an overview of biomedical applications. *J. Controlled Release* **2012**, *161*, 505−522.

(3) Wischke, C.; Schwendeman, S. P. Principles of encapsulating hydrophobic drugs in PLA/PLGA microparticles. *Int. J. Pharm.* **2008**, *364*, 298−327.

(4) Yu, L.; Zhang, Z.; Ding, J. Influence of LA and GA sequence in the PLGA block on the properties of thermogelling PLGA-PEG-PLGA block copolymers. *Biomacromolecules* **2011**, *12*, 1290−1297.

(5) Cho, H.; Gao, J.; Kwon, G. S. PEG-b-PLA micelles and PLGA-b-PEG-b-PLGA sol-gels for drug delivery. *J. Controlled Release* **2016**, *240*, 191−201.

(6) Siepmann, F.; Siepmann, J.; Walther, M.; MacRae, R. J.; Bodmeier, R. Polymer blends for controlled release coatings. *J. Controlled Release* **2008**, *125*, 1−15.

(7) Manca, M. L.; Loy, G.; Zaru, M.; Fadda, A. M.; Antimisiaris, S. G. Release of rifampicin from chitosan, PLGA and chitosan-coated PLGA microparticles. *Colloids Surf., B* **2008**, *67*, 166−170.

(8) Jose, M.; Thomas, V.; Johnson, K.; Dean, D.; Nyairo, E. Aligned PLGA/HA nanofibrous nanocomposite scaffolds for bone tissue engineering. *Acta Biomater.* **2009**, *5*, 305−315.

(9) Liu, Y.; Li, K.; Liu, B.; Feng, S.-S. A strategy for precision engineering of nanoparticles of biodegradable copolymers for quantitative control of targeted drug delivery. *Biomaterials* **2010**, *31*, 9145−9155.

(10) Xu, Q.; Ensign, L. M.; Boylan, N. J.; Schön, A.; Gong, X.; Yang, J.-C.; Lamb, N. W.; Cai, S.; Yu, T.; Freire, E.; Hanes, J. Impact of Surface Polyethylene Glycol (PEG) Density on Biodegradable Nanoparticle Transport in Mucus ex Vivo and Distribution in Vivo. *ACS Nano* **2015**, *9*, 9217−9227.

(11) Khalil, N. M.; Nascimento, T. C. F. d.; Casa, D. M.; Dalmolin, L. F.; Mattos, A. C. d.; Hoss, I.; Romano, M. A.; Mainardes, R. M. Pharmacokinetics of curcumin-loaded PLGA and PLGA-PEG blend nanoparticles after oral administration in rats. *Colloids Surf., B* **2013**, *101*, 353−360.

(12) Key, J.; Palange, A. L.; Gentile, F.; Aryal, S.; Stigliano, C.; Di Mascolo, D.; De Rosa, E.; Cho, M.; Lee, Y.; Singh, J.; Decuzzi, P. Soft Discoidal Polymeric Nanoconstructs Resist Macrophage Uptake and Enhance Vascular Targeting in Tumors. *ACS Nano* **2015**, *9*, 11628−11641.

(13) Palomba, R.; Palange, A. L.; Rizzuti, I. F.; Ferreira, M.; Cervadoro, A.; Barbato, M. G.; Canale, C.; Decuzzi, P. Modulating Phagocytic Cell Sequestration by Tailoring Nanoconstruct Softness. *ACS Nano* **2018**, *12*, 1433−1444.

(14) Behrens, A. M.; Lee, N. G.; Casey, B. J.; Srinivasan, P.; Sikorski, M. J.; Daristotle, J. L.; Sandler, A. D.; Kofinas, P. Biodegradable-polymer-blend-based surgical sealant with body-temperature-mediated adhesion. *Adv. Mater.* **2015**, *27*, 8056−8061.

(15) Kang, E.; Robinson, J.; Park, K.; Cheng, J.-X. Paclitaxel distribution in poly (ethylene glycol)/poly (lactide-co-glycolic acid) blends and its release visualized by coherent anti-Stokes Raman scattering microscopy. *J. Controlled Release* **2007**, *122*, 261−268.

(16) Ghobadi, E.; Heuchel, M.; Kratz, K.; Lendlein, A. Atomistic Simulation of the Shape-Memory Effect in Dry and Water Swollen Poly [(rac-lactide)-co-glycolide] and Copolyester Urethanes Thereof. *Macromol. Chem. Phys.* **2014**, *215*, 65−75.

(17) Horta, B. A. C.; Merz, P. T.; Fuchs, P. F. J.; Dolenc, J.; Riniker, S.; Hünenberger, P. H. A GROMOS-compatible force field for small organic molecules in the condensed phase: The 2016H66 parameter set. *J. Chem. Theory Comput.* **2016**, *12*, 3825−3850.

(18) Horta, B. A. C.; Fuchs, P. F. J.; van Gunsteren, W. F.; Hünenberger, P. H. New interaction parameters for oxygen compounds in the GROMOS force field: Improved pure-liquid and solvation properties for alcohols, ethers, aldehydes, ketones, carboxylic acids, and esters. *J. Chem. Theory Comput.* **2011**, *7*, 1016−1031.

(19) Fuchs, P. F. J.; Hansen, H. S.; Hünenberger, P. H.; Horta, B. A. C. A GROMOS parameter set for vicinal diether functions: properties of polyethyleneoxide and polyethyleneglycol. *J. Chem. Theory Comput.* **2012**, *8*, 3943−3963.

(20) Dechy-Cabaret, O.; Martin-Vaca, B.; Bourissou, D. Controlled ring-opening polymerization of lactide and glycolide. *Chem. Rev.* **2004**, *104*, 6147−6176.

(21) Nazarychev, V. M.; Lyulin, A. V.; Larin, S. V.; Gurtovenko, A. A.; Kenny, J. M.; Lyulin, S. V. Molecular dynamics simulations of uniaxial deformation of thermoplastic polyimides. *Soft Matter* **2016**, *12*, 3972−3981.

(22) Walkenhorst, R.; Selser, J. C.; Piet, G. Long-ranged relaxations in poly (ethylene oxide) melts: evidence for network behavior. *J. Chem. Phys.* **1998**, *109*, 11043−11050.

(23) Shmool, T. A.; Zeitler, J. A. Insights into the Structural Dynamics of PLGA at Terahertz Frequencies. **2018**, ChemRxiv.

(24) Glova, A. D.; Falkovich, S. G.; Dmitrienko, D. I.; Lyulin, A. V.; Larin, S. V.; Nazarychev, V. M.; Karttunen, M.; Lyulin, S. V. Scale-dependent miscibility of polylactide and polyhydroxybutyrate: molecular dynamics simulations. *Macromolecules* **2017**, *51*, 552−563.

(25) Hess, B.; Kutzner, C.; van der Spoel, D.; Lindahl, E. GROMACS 4: Algorithms for Highly Efficient, Load-Balanced, and Scalable Molecular Simulation. *J. Chem. Theory Comput.* **2008**, *4*, 435−447.

(26) Berendsen, H. J. C.; Postma, J. P. M.; van Gunsteren, W. F.; DiNola, A.; Haak, J. R. Molecular dynamics with coupling to an external bath. *J. Chem. Phys.* **1984**, *81*, 3684−3690.
(27) Hockney, R. W.; Goel, S. P.; Eastwood, J. W. Quiet high-resolution computer models of a plasma. *J. Comput. Phys.* **1974**, *14*, 148−158.
(28) Bussi, G.; Donadio, D.; Parrinello, M. Canonical sampling through velocity rescaling. *J. Chem. Phys.* **2007**, *126*, 014101.
(29) Parrinello, M.; Rahman, A. Polymorphic transitions in single crystals: A new molecular dynamics method. *J. Appl. Phys.* **1981**, *52*, 7182−7190.
(30) Gonçalves, Y. M. H.; Senac, C.; Fuchs, P. F. J.; Hünenberger, P. H.; Horta, B. A. C. Influence of the Treatment of Nonbonded Interactions on the Thermodynamic and Transport Properties of Pure Liquids Calculated Using the 2016H66 Force Field. *J. Chem. Theory Comput.* **2019**, *15*, 1806−1826.
(31) Barton, A. F. M. Solubility parameters. *Chem. Rev.* **1975**, *75*, 731−753.
(32) Hildebrand, J. H. SOLUBILITY. *J. Am. Chem. Soc.* **1916**, *38*, 1452−1473.
(33) Belmares, M.; Blanco, M.; Goddard, W. A., Iii; Ross, R. B.; Caldwell, G.; Chou, S.-H.; Pham, J.; Olofson, P. M.; Thomas, C. Hildebrand and Hansen solubility parameters from molecular dynamics with applications to electronic nose polymer sensors. *J. Comput. Chem.* **2004**, *25*, 1814−1826.
(34) Astete, C. E.; Sabliov, C. M. Synthesis and characterization of PLGA nanoparticles. *J. Biomater. Sci., Polym. Ed.* **2006**, *17*, 247−289.
(35) Rubinstein, M.; Colby, R. H. *Polymer Physics*; Oxford University Press: New York, 2003; Vol. *23*.
(36) Moga, S. A.; Goga, N.; Hadar, A. Developing a novel algorithm for the computation of poisson's ratio using molecular dynamics for polymers. *Univ. "Politeh." Bucharest, Sci. Bull., Ser. B* **2016**, *78*, 129−136.
(37) Pappalardo, M.; Milardi, D.; Grasso, D.; La Rosa, C. Phase behaviour of polymer-grafted DPPC membranes for drug delivery systems design. *J. Therm. Anal. Calorim.* **2005**, *80*, 413−418.
(38) Jaeger, G. The Ehrenfest classification of phase transitions: introduction and evolution. *Arch. Hist. Exact Sci.* **1998**, *53*, 51−81.
(39) Stanley, H. E.; Ahlers, G. Introduction to phase transitions and critical phenomena. *Phys. Today* **1973**, *26*, 71.
(40) Lubchenko, V. Theory of the structural glass transition: A pedagogical review. *Adv. Phys.* **2015**, *64*, 283−443.
(41) Romanucci, V.; Milardi, D.; Campagna, T.; Gaglione, M.; Messere, A.; D'Urso, A.; Crisafi, E.; La Rosa, C.; Zarrelli, A.; Balzarini, J.; Di Fabio, G. Synthesis, biophysical characterization and anti-HIV activity of d (TG3AG) quadruplexes bearing hydrophobic tails at the 5′-end. *Bioorg. Med. Chem.* **2014**, *22*, 960−966.
(42) Grunewald, F.; Rossi, G.; de Vries, A. H.; Marrink, S. J.; Monticelli, L. Transferable MARTINI Model of Poly(ethylene Oxide). *J. Phys. Chem. B* **2018**, *122*, 7436−7449.
(43) De Gennes, P.-G.; Gennes, P.-G. *Scaling Concepts in Polymer Physics*; Cornell University Press, 1979.
(44) Caré, B. R.; Emeriau, P.-E.; Cortini, R.; Victor, J.-M. Chromatin epigenomic domain folding: size matters. *AIMS Biophys.* **2015**, *2*, 517.
(45) Lesage, A.; Dahirel, V.; Victor, J.-M.; Barbi, M. Polymer coil−globule phase transition is a universal folding principle of Drosophila epigenetic domains. *Epigenet. Chromatin* **2019**, *12*, 1−15.
(46) Körber, M. PLGA erosion: solubility-or diffusion-controlled? *Pharm. Res.* **2010**, *27*, 2414−2420.
(47) Pourasghar, M.; Koenneke, A.; Meiers, P.; Schneider, M. Development of a fast and precise method for simultaneous quantification of the PLGA monomers lactic and glycolic acid by HPLC. *J. Pharm. Anal.* **2019**, *9*, 100−107.
(48) Eser, H.; Tihminlioglu, F. Determination of thermodynamic and transport properties of solvents and non solvents in poly (L-lactide-co-glycolide). *J. Appl. Polym. Sci.* **2006**, *102*, 2426−2432.
(49) Allegra, G.; Ganazzoli, F.; Bontempelli, S. Good-and bad-solvent effect on the rotational statistics of a long chain molecule. *Comput. Theor. Polym. Sci.* **1998**, *8*, 209−218.
(50) Mark, J. E.; Flory, P. J. The configuration of the polyoxyethylene chain. *J. Am. Chem. Soc.* **1965**, *87*, 1415−1423.
(51) Saeed, K.; ISHAQ, M.; ILYAS, M. Preparation, morphology, and thermomechanical properties of coal ash/polyethylene oxide composites. *Turk. J. Chem.* **2011**, *35*, 237−243.
(52) Nie, H.-Y.; Motomatsu, M.; Mizutani, W.; Tokumoto, H. Local modification of elastic properties of polystyrene−polyethyleneoxide blend surfaces. *J. Vac. Sci. Technol., B: Microelectron. Nanometer Struct.–Process., Meas., Phenom.* **1995**, *13*, 1163−1166.
(53) Shirazi, R. N.; Aldabbagh, F.; Erxleben, A.; Rochev, Y.; McHugh, P. Nanomechanical properties of poly (lactic-co-glycolic) acid film during degradation. *Acta Biomater.* **2014**, *10*, 4695−4703.
(54) Astafyeva, K.; Thomas, J.-L.; Coulouvrat, F.; Guédra, M.; Diou, O.; Mousnier, L.; Tsapis, N.; Urbach, W.; Taulier, N. Properties of theranostic nanoparticles determined in suspension by ultrasonic spectroscopy. *Phys. Chem. Chem. Phys.* **2015**, *17*, 25483−25493.
(55) Dumitru, A. C.; Espinosa, F. M.; Garcia, R.; Foschi, G.; Tortorella, S.; Valle, F.; Dallavalle, M.; Zerbetto, F.; Biscarini, F. In situ nanomechanical characterization of the early stages of swelling and degradation of a biodegradable polymer. *Nanoscale* **2015**, *7*, 5403−5410.
(56) Abadi, M.; Serag, M. F.; Habuchi, S. Entangled polymer dynamics beyond reptation. *Nat. Commun.* **2018**, *9*, 5098.
(57) Hildebrand, J.; Scott, R. *The Solubility of Nonelectrolytes*; Reinhold Pub. Co.: New York, 1950; p 3.
(58) Biroa, J.; Zeman, L.; Patterson, D. Prediction of the X Parameter by the solubility parameter and corresponding states theories. *Macromolecules* **1971**, *4*, 30−35.
(59) Chen, X.; Yuan, C.; Wong, C. K. Y.; Zhang, G. Molecular modeling of temperature dependence of solubility parameters for amorphous polymers. *J. Mol. Model.* **2012**, *18*, 2333−2341.
(60) Marciniak, A. The Hildebrand solubility parameters of ionic liquids—part 2. *Int. J. Mol. Sci.* **2011**, *12*, 3553−3575.
(61) Coleman, M. M.; Serman, C. J.; Bhagwagar, D. E.; Painter, P. C. A practical guide to polymer miscibility. *Polymer* **1990**, *31*, 1187−1203.
(62) Steele, T. W. J.; Huang, C. L.; Widjaja, E.; Boey, F. Y. C.; Loo, J. S. C.; Venkatraman, S. S. The effect of polyethylene glycol structure on paclitaxel drug release and mechanical properties of PLGA thin films. *Acta Biomater.* **2011**, *7*, 1973−1983.
(63) Evrova, O.; Hosseini, V.; Milleret, V.; Palazzolo, G.; Zenobi-Wong, M.; Sulser, T.; Buschmann, J.; Eberli, D. Hybrid randomly electrospun poly (lactic-co-glycolic acid): poly (ethylene oxide)-(PLGA: PEO) fibrous scaffolds enhancing myoblast differentiation and alignment. *ACS Appl. Mater. Interfaces* **2016**, *8*, 31574−31586.

https://dx.doi.org/10.1021/acs.macromol.0c00110
Macromolecules 2020, 53, 3643−3654